Effect of heat treatment paths on the aging and rejuvenation of metallic glasses

Suyue Yuan [1,2] Aoyan Liang [1] Chang Liu,[1] Liang Tian,[3] Normand Mousseau [4] and Paulo S. Branicio [1,*]

[1]*Mork Family Department of Chemical Engineering and Materials Science, University of Southern California, Los Angeles, California 90089, USA*

[2]*Materials Science Division, Lawrence Livermore National Laboratory, Livermore, California 94550, USA*

[3]*Frontier Institute of Science and Technology (FIST), Xi'an Jiaotong University, Xi'an, Shaanxi 710049, China*

[4]*Département de Physique, Université de Montréal, C.P. 6128, succ. Centre-ville, Montreal, PQ, Canada*

(Received 29 April 2023; accepted 21 November 2023; published 18 December 2023)

This study explores the influence of heat treatment paths on the structural relaxation of metallic glasses (MGs) in the regime of fast dynamics. We create MG samples using various quenching rates, from 10^9 to 10^{11} K/s, and expose these samples to near-T_g heat treatments with assorted combinations of heating (cooling) rates, from 5×10^{10} to 5×10^{12} K/s, and annealing durations, from 10 ps to 10 ns. Results show that the effect of the heating rate is intricately tied to the initial structure of the MG, while a decrease in the cooling rate invariably intensifies the aging process. Extending the annealing duration may induce either aging or rejuvenation, subject to the specific thermal history. To interpret these findings, we hypothesize that the memory effect, governed by the activation and annihilation of reversible and irreversible flow units, underpins the rejuvenation-aging competition in MGs. Moreover, we suggest viewing the cooling stage as an annealing phase controlled by gradient temperature and fine-tuning its rate to achieve the targeted active-flow unit distributions. This study illuminates the role of fast dynamics during the glass relaxation process and offers practical strategies for tailoring heat treatments to optimize MG structures and mechanical performance.

DOI: 10.1103/PhysRevMaterials.7.123603

I. INTRODUCTION

Metallic glasses (MGs) are recognized for their superior properties compared to traditional crystalline metals, including exceptional strength, elasticity, and resistance to corrosion [1–3]. Moreover, their significant thermal stability within the wide supercooled-liquid region allows for the implementation of heat treatment and thermoplastic processing [4]. These unique characteristics render them ideal candidates for a variety of engineering applications. However, MGs' strain-softening tendency results in limited plasticity at ambient temperatures making them prone to catastrophic failure, which consequently hampers their utilization as structural materials [2,4]. Considering MGs' inherent transition from a supercooled-liquid metastable equilibrium state to a nonequilibrium glass state [5,6], a typical strategy for tailoring their physical properties involves inducing aging or rejuvenation through different thermal and mechanical treatments [7–11].

Forecasting the extent of aging and rejuvenation processing of MGs proved challenging [8–10,12]. The underlying mechanisms responsible for the structural relaxation remain puzzling, primarily owing to the multifaceted relaxation modes exhibited by MGs at varying temperatures. These modes include α relaxation, β relaxation, γ relaxation, and fast-cage dynamics. Each mode corresponds to different relaxation times, vibrational frequencies, and activation temperatures, all of which are intricately linked with the dynamics and structural heterogeneities inherent in MGs [9,13–16]. Even within a relaxation mode, there can be distinct parts. For instance, Zhao *et al.* observed a distinctive endothermic peak in MGs following extensive sub-T_g annealing and attributed it to the reversible part of the β relaxation [17]. Wang *et al.* reported an interesting rejuvenation phenomenon in Cu-Zr MGs, where reheating an initially aged sample to a higher annealing temperature during a second annealing process resulted in an enhanced degree of rejuvenation compared to the original rejuvenated sample at the same temperature [10]. Recently, Sun *et al.* revealed a novel relaxation mechanism in MGs where relaxation and dynamics at low temperatures follow a unique stretched exponential decay. This is distinct from that of a supercooled liquid, and such aging dynamics originate from energy release typical of out-of-equilibrium systems, which manifest as defect elimination through localized atomic strains [18]. However, the current comprehension of relaxation behavior, especially regarding fast dynamics and the memory effect in MG structures during heat treatment, remains incomplete. Specifically, the reversible and irreversible structural evolutions induced by relaxation behavior within the fast-dynamics regime, which operates on a nanosecond timescale, are yet to be fully understood.

Classical molecular dynamics (MD) simulations have elucidated the correlation between structure and properties in MGs [11,19–21]. However, these simulations, due to computational constraints, usually employ rapid cooling procedures with extraordinarily high cooling rates of 10^9–10^{13} K/s, far exceeding the standard experimental cooling rates for melt spinning, typically around 10^5–10^6 K/s. At such high cooling

*branicio@usc.edu

rates, crystallization can be kinetically inhibited, leading to an under-relaxed glassy structure. To narrow the discrepancy between samples produced by MD simulations (spanning up to microseconds) and experimentally relaxed MG structures, systematic control of annealing temperatures and times for heat treating as-cast samples has become a research focus. For instance, Zhang *et al.* proposed fabricating CuZr MG using a sub-T_g annealing process to achieve structures with lower potential energy and enhanced short-range icosahedral order, comparable to samples created at slower cooling rates [12]. Şopu *et al.* suggested annealing MGs above T_g to reduce the computational time needed for achieving well-relaxed glasses [22]. While simulation works provide atomic-level insights into the structural relaxation of MGs, particularly in the fast-dynamics regime, the intricate kinetics and resultant structures under different heat treatment paths remain elusive.

In this study, we employ MD simulations to examine the structural dynamics of MGs under different heat treatment paths. We create MGs with diverse initial structures by employing different quenching rates, and subject them to unique heat treatment paths. Subsequent tensile loading simulations on these MG samples enable us to explore their structural evolution from the perspective of structural-property correlations. Our results reveal that heating and cooling rates impart distinct impacts on the structural relaxation of MGs, thereby resulting in their different mechanical performance. The influence of the heating rate is heavily contingent on the MG's initial structure, while a decrease in cooling rate invariably enhances the aging effect in MGs. Extending the duration of annealing can either induce aging or rejuvenation, depending on the prior thermal history of the sample. These results are further explained through the analysis of the fast dynamics and memory effect associated with flow units in MGs.

II. METHODOLOGY

We simulate CuZr alloys, an MG archetype, using the Large-scale Atomic/Molecular Massively Parallel Simulator (LAMMPS) package [23].The interactions are characterized by an embedded-atom method potential [24]. To fabricate the initial MG structures, we melt a $Cu_{64}Zr_{36}$ alloy sample containing ∼16 000 atoms and thermalize it at 2000 K for 0.2 ns. This melt configuration serves as the foundational structure for generating diverse amorphous samples. These samples are created by cooling the structure down to 1 K at quenching rates (r_q) of 10^9, 10^{10}, and 10^{11} K/s, respectively, while maintaining zero external pressure. Throughout the quenching and heat treatment simulations, we employ periodic boundary conditions in all directions and a 2-fs time step. The resulting glass transition temperatures, T_g, for the MGs prepared at each quenching rate fall within the range of 790–810 K. Given the temperature window for structural evolution in MGs, we designated a temperature slightly above T_g, i.e., 850 K, as the subsequent annealing temperature. This scheme allows for some degree of structural evolution to be observed within the confined simulation time, while preserving the glassy structure. Further insights into structural evolution as a function of temperature can be explored in Supplemental Material, Figs. S1 and S2 [25]. Following the creation of as-cast MG samples, a near-T_g annealing treatment is performed. This procedure involves reheating the samples from 1 to 850 K at a rate of 5×10^{10}, 5×10^{11}, or 5×10^{12} K/s, equilibrating at this temperature for 10, 100, 1000, or 10 000 ps, and then cooling them down to 1 K at a rate of 5×10^{10}, 5×10^{11}, or 5×10^{12} K/s. The selected annealing times aim to capture the transition from relaxation to diffusion behavior in MGs at the annealing temperature, which is guided by the mean-square displacement of atoms in MGs at the annealing temperature, as detailed in Supplemental Material, Fig. S5. In the end, the thermal history of these samples is characterized by a combination of different heating rates (r_h), annealing times, and cooling rates (r_c). Following the generation and structure analysis of MGs treated with various thermal histories, we proceed to conduct tensile loading simulations on these samples to explore the structural-property correlations. Initially, the MGs treated with different thermal histories are replicated to form a larger system size of $38 \times 57 \times 6.4\,\text{nm}^3$, comprising 86 400 atoms. Subsequently, tensile loading simulations are performed at a constant strain rate of $10^8\,\text{s}^{-1}$, with temperature controlled at 50 K and zero isotropic pressure, utilizing the *NPT* ensemble. During the simulation, periodic boundary conditions in all directions and a 1-fs time step are applied.

III. RESULTS

Data of MGs prepared with 108 distinct thermal history paths are collected, each determined by combining different quenching rates, heating rates, annealing durations, and cooling rates. We present our statistical findings using box-and-whisker plots, as shown in Fig. 1, which offers a clear representation of the data distribution, including the median, quartiles, and range. The whiskers extend from the box to the minimum and maximum data points within a 1.5 interquartile range. Outliers beyond this range are indicated. The results are organized based on the quenching rates used to create the initial MG structures, with the heat treatment procedure encompassing all possible combinations of three heating rates, four annealing durations, and three cooling rates. The heating and cooling rates are then translated into corresponding durations: heating (cooling) rates of 5×10^{10}, 5×10^{11}, and 5×10^{12} K/s correspond to heating (cooling) times of 16 000, 1600, and 160 ps, respectively.

Figures 1(a)–1(c) display the variation in potential energy, ΔPE, which is determined by comparing the potential energy per atom (PE) of the as-cast MG sample without any heat treatment with that of the same sample following a complete heat treatment process. A negative ΔPE indicates aging, while a positive ΔPE implies rejuvenation of the MG. Notably, the influence of heating time on the ΔPE is highly dependent on the initial MG structure and does not demonstrate a simple monotonic relationship, as seen in Fig. 1(a). Surprisingly, for MGs prepared at slower quenching rates, extending the annealing time leads to a significant increase in ΔPE, and the extent of this increase is linked to the initial MG structure, as shown in Fig. 1(b). For MGs prepared at a faster quenching rate, the effect of the annealing time on ΔPE is more complex and does not follow a clear trend. Notably, increasing the cooling time consistently reduces the ΔPE, thereby enhancing the aging effect in MGs, irrespective of the variations in heating, annealing times, or initial structures, as depicted in

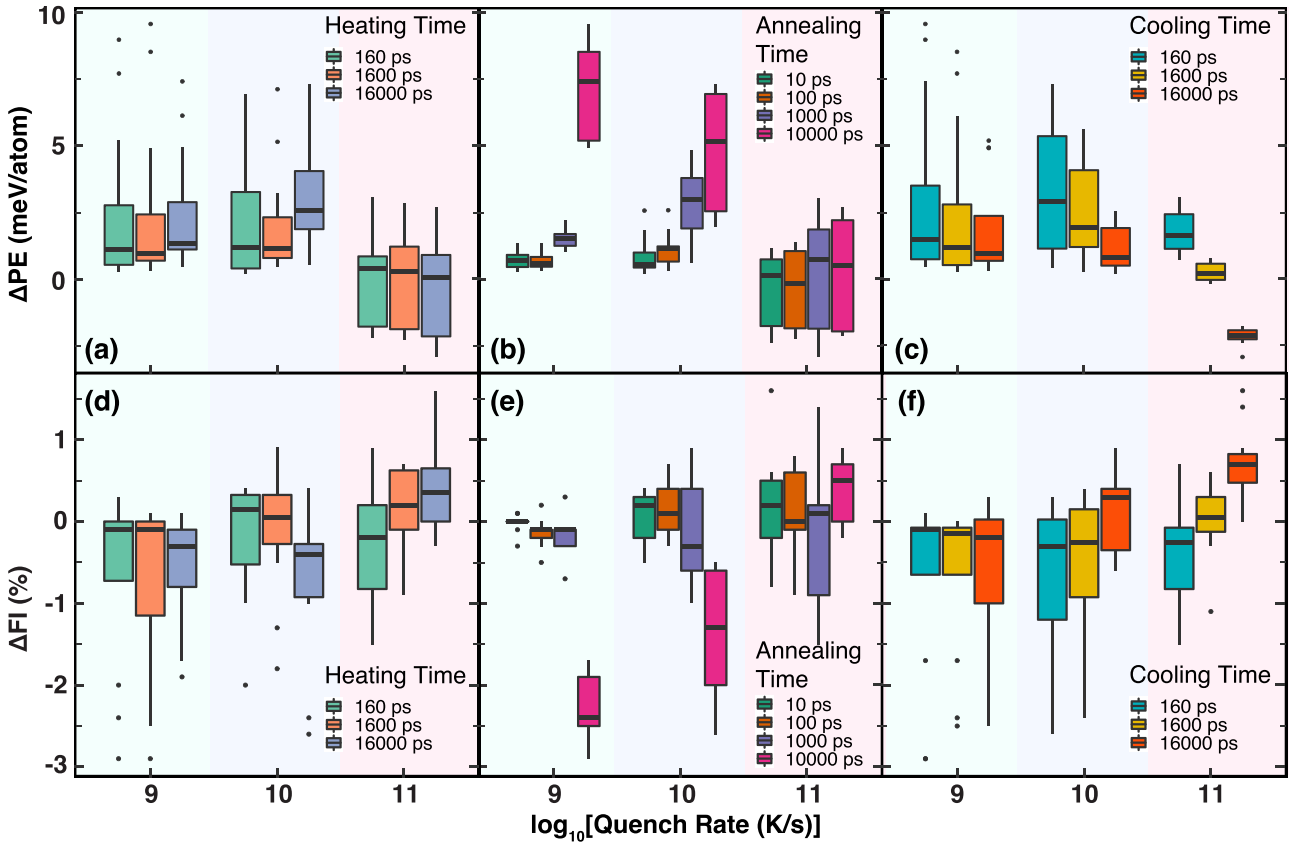

FIG. 1. State transitions of metallic glasses (MGs) following various heat treatment paths. (a)–(c) Potential-energy variation (ΔPE) and (d)–(f) full icosahedra concentration variation (ΔFI) in MGs generated with different quenching rates, grouped by the heating time, annealing time, and cooling time, respectively. Whiskers extend from the box to the minimum and maximum data points within 1.5 times the interquartile range.

Fig. 1(c). The impacts of heating, annealing, cooling, and total time (the sum of all three) on ΔPE are further quantified using Spearman's correlation function, which evaluates monotonic relationships between two variables. As shown in Table I, the heating time exhibits a weak correlation with ΔPE and can induce either aging or rejuvenation effects, depending on the initial MG structure. The annealing time has a robust positive correlation with ΔPE and tends to promote the rejuvenation of MGs that have a more compact initial structure. Conversely, the cooling time consistently exhibits a negative relationship with ΔPE and has a pronounced aging effect on MGs with loosely packed structures.

TABLE I. Spearman's correlation coefficients between state parameters changes (ΔPE, ΔFI) in MGs and heat treatment parameters.

	Heating time	Annealing time	Cooling time	Total time
ΔPE (for all r_q)	0.105	0.538	−0.439	−0.055
ΔPE ($r_q = 10^9$ K/s)	0.138	0.844	−0.187	0.266
ΔPE ($r_q = 10^{10}$ K/s)	0.265	0.758	−0.468	0.060
ΔPE ($r_q = 10^{11}$ K/s)	−0.098	0.182	−0.937	−0.652
ΔFI (for all r_q)	−0.007	−0.379	0.356	0.116
ΔFI ($r_q = 10^9$ K/s	−0.113	−0.763	0.023	−0.291
ΔFI ($r_q = 10^{10}$ K/s	−0.266	−0.615	0.411	−0.110
ΔFI ($r_q = 10^{11}$ K/s)	0.366	0.104	0.693	0.766

A fundamental aspect of short-range order (SRO) in CuZr MGs involves the prevalence of full icosahedra (FI) or icosahedral-like atomic clusters. A higher fraction of FI typically suggests a more solidlike structure and a lower energy state, while a lower fraction of FI implies a more liquidlike structure and a higher energy state [26–29]. Figures 1(d)–1(f) illustrate the variations in FI within MG samples subject to different heat treatment paths, with trends in ΔFI aligning with our earlier discussions regarding ΔPE. The corresponding Spearman correlation coefficients are also compiled and presented in Table I. The influence of heating and annealing time on ΔFI is dependent on the initial MG structure. Increasing their duration decreases the FI fraction in MGs produced at slower quenching rates and increases the fraction in MGs produced at faster rates. In contrast, extended cooling times consistently promote an increase in the FI fraction.

Notably, post-heat treatment, particularly for MGs created with a 10^9 K/s quenching rate (see Fig. 1), samples exhibit concurrent positive ΔPE and ΔFI values, indicating an enhanced level of SRO in a rejuvenated MG. We suggest that the observed decoupling of ΔPE and ΔFI can be rationalized by understanding that the enhancement of SRO in an MG structure does not necessarily result in a decrease in the

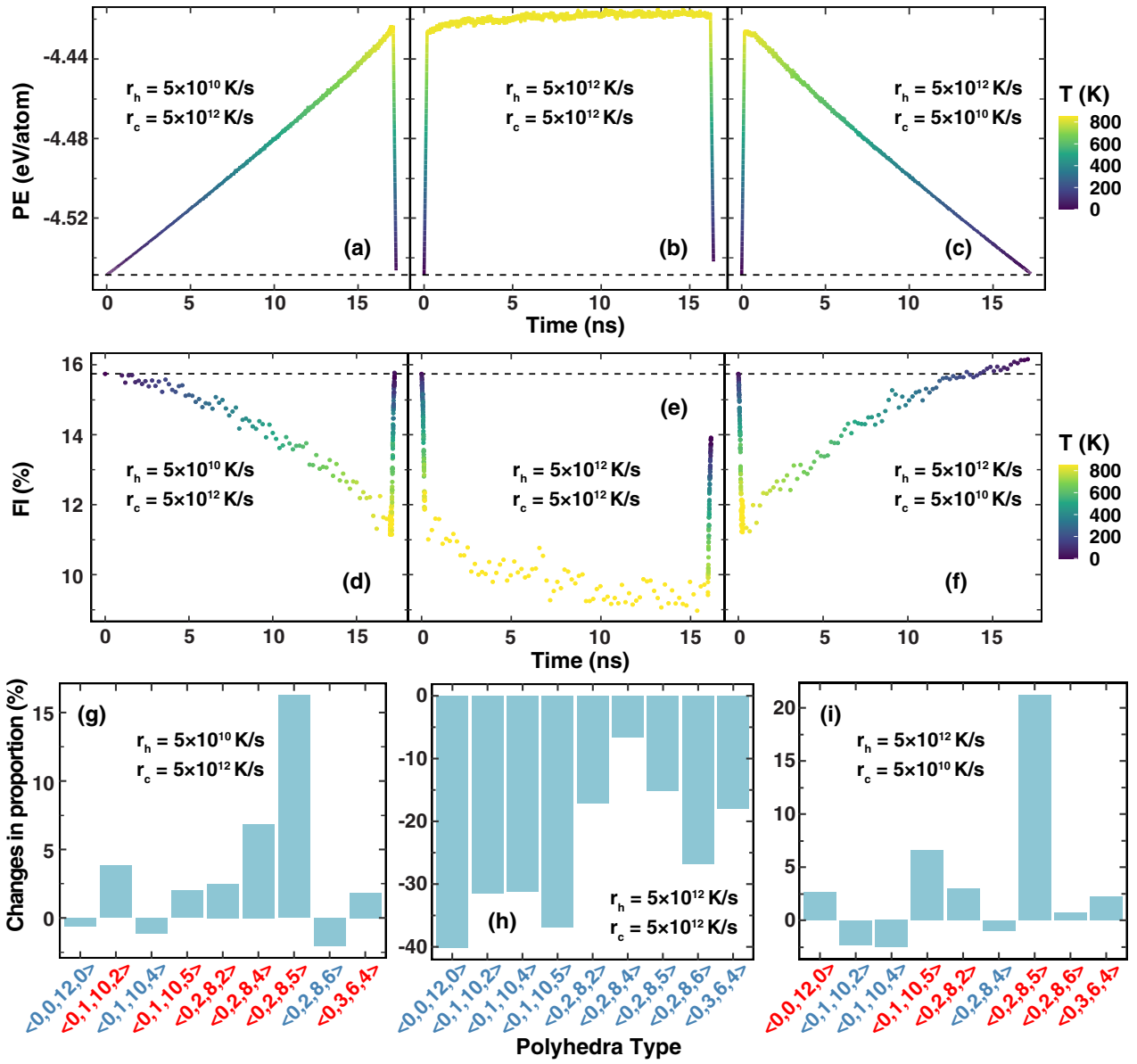

FIG. 2. Structural evolution of MGs under varying heat treatment paths. (a)–(c) PE, (d)–(f) FI concentration, and (g)–(i) Polyhedra distribution evolutions in MGs undergo heat treatment with varying combinations of heating and cooling rates. All samples are generated at quenching rate of 10^{10} K/s and subjected to heat treatments of equal duration. The dashed line indicates the measurements of PE and FI concentrations in MGs at 1 K before heat treatment. The curves are color coded based on the instantaneous sample temperature. The polyhedra types are color coded based on the positive or negative changes.

energy state. This viewpoint can be interpreted in terms of the potential-energy landscape (PEL) [30], where a specific structural evolution corresponds to the transitions between metabasins or subbasins confined within a metabasin. In this framework, the enhanced ΔPE could arise from a lower medium-range order (MRO) of MGs [29]. This can also be understood from the perspective of atomic motion. As reported by Giordano and Ruta, fast dynamical aging is associated not only with the elimination of structural defects, but also with a more rapid process of medium-range ordering [6]. Therefore, there may exist a competitive interplay between the evolution of SRO and MRO that plays a key role in determining the final energy state of MGs.

To further our understanding of the structural evolution of MGs under varying heat treatment paths, especially concerning heating and cooling rates, we start with the MG sample produced with a quenching rate of 10^{10} K/s. We then produced samples applying heat treatments of equal duration. Figures 2(a) and 2(d) depict the case in which the sample is heated from 1 to 850 K at a rate of 5×10^{10} K/s, held for 100 ps, then cooled to 1 K at a rate of 5×10^{12} K/s. The dashed line represents the measurements of PE and FI% in as-cast MGs. One can see minor increase in PE and nearly no change in FI% compared with the as-cast sample. In contrast, Figs. 2(b) and 2(e) represent the sample heated at a rate of 5×10^{12} K/s, held for ∼16 ns, and then cooled to 1 K at a

rate of 5×10^{12} K/s. While the PE sees only a slight increase compared with the as-cast MG (dashed line), a noticeable decrease in the FI concentration from 15.7 to 14% is observed. Meanwhile, Figs. 2(c) and 2(f) show the sample heated at a rate of 5×10^{12} K/s, held for 100 ps, and then cooled to 1 K at a rate of 5×10^{10} K/s. Here, negligible change in PE and a significant increase in FI% from 15.7 to 16.2% are observed. These observations suggest that the cooling stage in the heat treatment process plays a crucial role in the structural evolution of MGs, though its impact may not be prominently reflected by the state energy. Slowing down the cooling process can boost the FI% of MGs more effectively than extending the heating or annealing period, considering that the total treatment time remains constant. More details regarding the variations in PE and FI% with temperature can be found in the Supplemental Material, Fig. S3.

Figures 2(g)–2(i) illustrate the shifts in polyhedra distribution, as determined by the Voronoi index, for better understanding the local structure evolution caused by heat treatment. The calculations are done by comparing the fractions of each type of polyhedra in the post-heat treatment MG sample with their initial proportions. Note that we do not discriminate based on the type of the center atom (Cu or Zr) in the polyhedra, and only the predominant polyhedra statistics is provided. A distinct divergence can be observed in the resulting structure spectra when the samples are subjected to different heat treatments. For instance, the sample subjected to an extended annealing period displays a substantial decrease in the fraction of all dominant polyhedra types, as seen in Fig. 2(h). The sample subjected to slower heating reveals a prominent increase (above 5%) in the fraction of ⟨0 2 8 4⟩ and ⟨0 2 8 5⟩-type polyhedra. On the other hand, the sample subjected to slower cooling display a considerable increase in the fractions of ⟨0 1 10 5⟩ and ⟨0 2 8 5⟩-type polyhedra. These findings confirm our previous hypothesis that by strategically allocating the heating, annealing, and cooling periods within a fixed total treatment time, it is possible to achieve considerably varied MG structures. Additionally, pair-distribution functions for MGs subjected to varying thermal histories are presented in Fig. S4 of the Supplemental Material. Although differences between MGs treated with a low cooling rate and a low heating rate are not apparent, they are readily distinguished from the MG treated with a longer annealing time, as evidenced by sharper and more segregated peaks.

In Fig. 3, we show the atomic displacement statistics during sample relaxation, which is achieved by computing the instantaneous difference between current and initial particle coordinates at the onset of annealing. Figure 3(a) shows the results obtained by heating MGs produced at a quenching rate of 10^{10} K/s to 850 K using two different heating rates, 5×10^{10} and 5×10^{12} K/s. These samples are then annealed over varying periods, ranging from 10 ps to 20 ns. For equilibration times less than 100 ps, the displacement magnitude stays below the average bond-length values (Cu–Cu: 2.6 Å, Cu–Zr: 2.8 Å, and Zr–Zr: 3.3 Å) for both heating rates. This suggests that the primary atomic displacement mode is largely confined within the "cage" [31–33]. However, when the relaxation time extends to 10 ns, the displacement distribution broadens and surpasses the average bond-length values. We

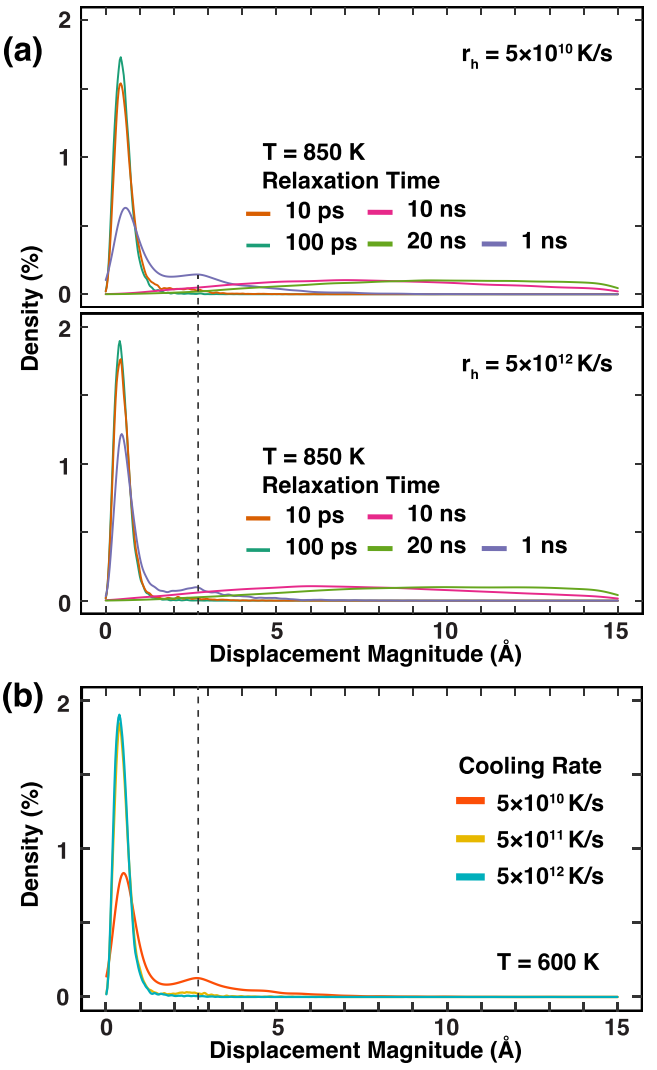

FIG. 3. Atomic displacement statistics in MGs subjected to varying heating and cooling rates. (a) MGs heated at different rates and annealed at 850 K for varying durations. (b) MGs initially heated to 850 K at a rate of 5×10^{11} K/s, followed by cooling to 600 K at assorted rates. The dashed line highlights the secondary peak.

pinpoint a critical relaxation time at 1 ns, where the disparity in atomic displacement between MGs treated with different heating rates is noticeable. Both curves present a secondary peak at ∼2.6 Å, with the MG heated at a slower rate containing a larger proportion of atoms at this peak. We employ the theory of fast-caged dynamics, which manifests within a temporal window that is shorter than β relaxation yet longer than the boson peak, to interpret these findings [34,35]. Initially, MG atoms are trapped within cages formed by adjacent atoms or clusters due to an anharmonic interatomic potential, thereby confining their motion to a limited configuration space. As relaxation time lengthens, fluctuations in atomic motions within the cages lead to the final escape and result in a different relaxation mode [9,36]. We propose that the cage radius can be estimated by identifying the second peak in the displacement magnitude distribution, which is the same as the average Cu–Cu bond length. Furthermore, when the MG is subjected to a slower heating rate, it transitions into a higher

energy state within the PEL, which promotes the release of atoms from their initial confined local arrangements, or their cages.

Similarly, Fig. 3(b) displays atomic displacement statistics obtained from MGs subjected to different cooling rates during heat treatment. Samples quenched at a rate of 10^{10} K/s are reheated to 850 K at a rate of 5×10^{11} K/s, then separately cooled to 600 K at rates of 5×10^{10}, 5×10^{11}, and 5×10^{12} K/s. The results are derived from the particles coordinates at 850 K and 600 K. The peaks of the 5×10^{11} and 5×10^{12} curves rapidly plummet to near zero within 2 Å, while the 5×10^{10} K/s curve slightly shifts towards larger values, revealing a second peak at ∼2.6 Å, in good agreement with the second peak position shown in Fig. 3(a). This reinforces our prior assumption that the emergence of the second peak can be ascribed to the cage-structure dynamics and is likely independent of temperature. Slower cooling rates in the MG heat treatment process cause a higher proportion of atoms to experience greater displacements, owing to an extended relaxation time required for transitioning from higher to lower energy states. Consequently, this results in fewer atoms being frozen in their loosely packed configurations.

The findings discussed earlier underscore the significant role that heat treatment cooling rates play in the behavior of MGs. We now turn our attention to studying the impact of the cooling rate on the energy states of MGs post-heat treatment. These energy states are associated with the process of structural relaxation, which is facilitated by atomic configuration transitions wherein atoms hop between two local energy minima separated by an energy barrier [30]. First, the MG samples are produced using a quenching rate of 10^{10} K/s. They are then heated from 1 K to 850 K at a rate of 5×10^{11} K/s, annealed for 100 ps, and cooled to 1 K at three different rates ($r_c = 5 \times 10^{10}$, 5×10^{11}, and 5×10^{12} K/s). The chosen annealing times aim to reflect the active annealing effect while mitigating intensive diffusion behavior in the MG, as indicated by Fig. S5 in the Supplemental Material. Next, the activation-relaxation technique (ART) nouveau method [37,38] is employed to explore the PEL of the MG structures by inspecting their local excitations [30,39]. For each MG system, we employ ten ART searches with different perturbation directions for 10 000 randomly selected atoms. After eliminating failed searches and duplicate events, we manage to pinpoint ∼2500 unique activations for each sample. Atoms involved in lower activation energy events suggest weaker bonding or a less densely packed local environment, while atoms in higher activation energy events indicate stronger bonding or a more densely packed local environment.

As depicted in Fig. 4(a), though the distribution curve peaks do not exhibit significant differences, discernible variations are observed in the proportions of events on two sides of the curve. In comparison to the as-cast curve, the curve representing $r_c = 5 \times 10^{10}$ K/s shows a larger number of events with higher activation energies and marginally fewer number of events with lower activation energies, indicating a more densely packed MG structure. In contrast, the curve for $r_c = 5 \times 10^{12}$ K/s reveals a wider dispersion, with an increase in the fractions of both lower and higher activation energy events, as marked by the dashed rectangular boxes positioned at two sides of the curves. This suggests that the fast cooling

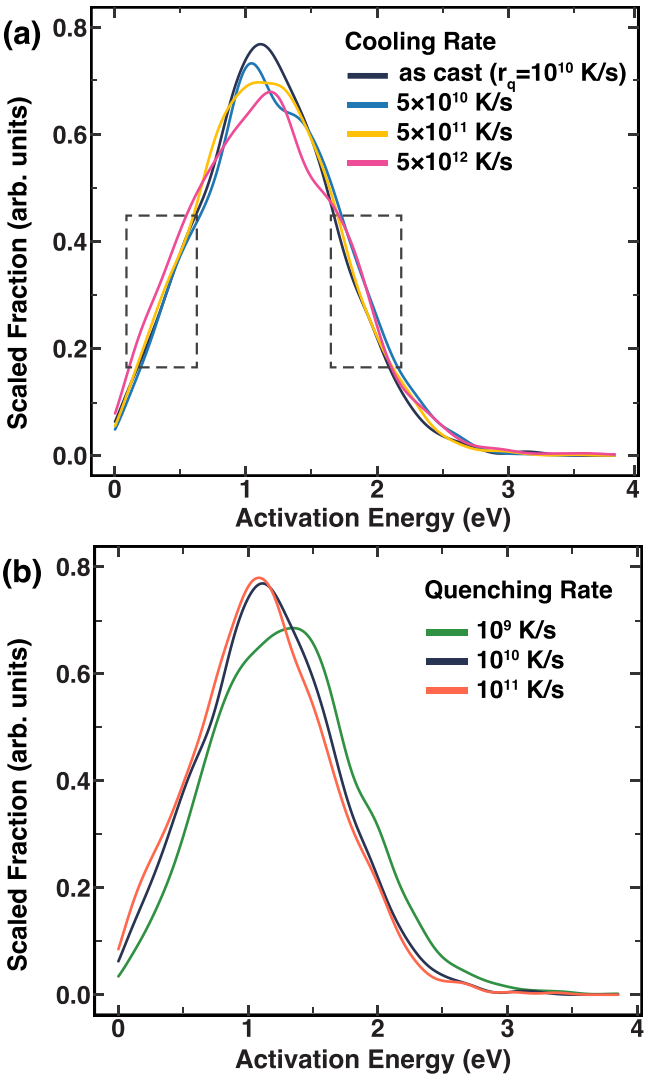

FIG. 4. Activation energy statistics of MGs following various heat treatment paths. (a) As-cast MG generated at a quenching rate of 10^{10} K/s and the same sample subjected to heat treatment using different cooling rates. The heat treatment process includes reheating the MG sample to 850 K at a rate of 5×10^{11} K/s, annealing for 100 ps, and subsequent cooling down to 1 K at rates of 5×10^{10}, 5×10^{11}, and 5×10^{12} K/s, respectively. The key differences among these samples are marked by the dashed rectangular boxes positioned at two sides of the curves. (b) As-cast MGs generated at a quenching rate of 10^{9}, 10^{10}, and 10^{11} K/s, respectively.

can result in a concurrent increase in both loosely packed and densely packed configurations, thereby manifesting structural heterogeneity across a length scale ranging from SRO to MRO in MGs.

For comparative purposes, Fig. 4(b) also displays the activation energy distributions of as-cast MG samples produced at different quenching rates ($r_q = 10^9$, 10^{10}, and 10^{11} K/s). A clear shift of the curve towards higher energy states can be observed as the quenching rate decreases, with a larger fraction of events having higher activation energies and a smaller fraction with lower energy states. This observation aligns with the case of applying a lower cooling-rate heat treatment and

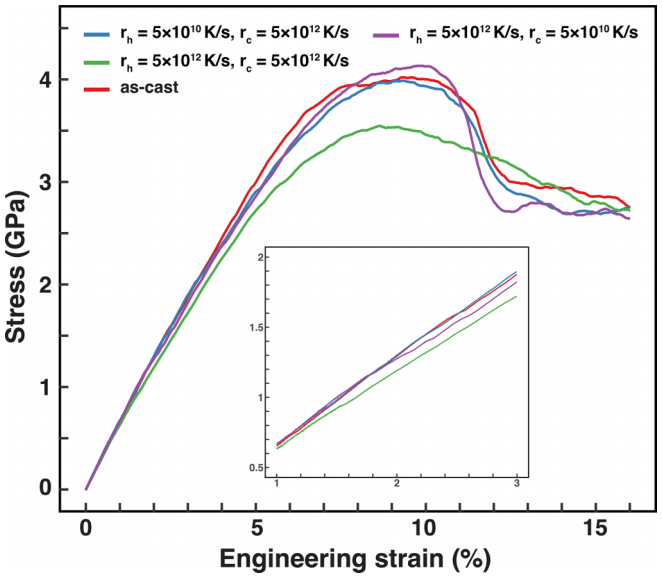

FIG. 5. Stress-strain curves of MGs under tensile loading. All samples are generated at a quenching rate of 10^{10} K/s. MGs subjected to heat treatment with varying combinations of heating and cooling rates undergo an equal total treatment duration. The inset emphasizes the elastic regime.

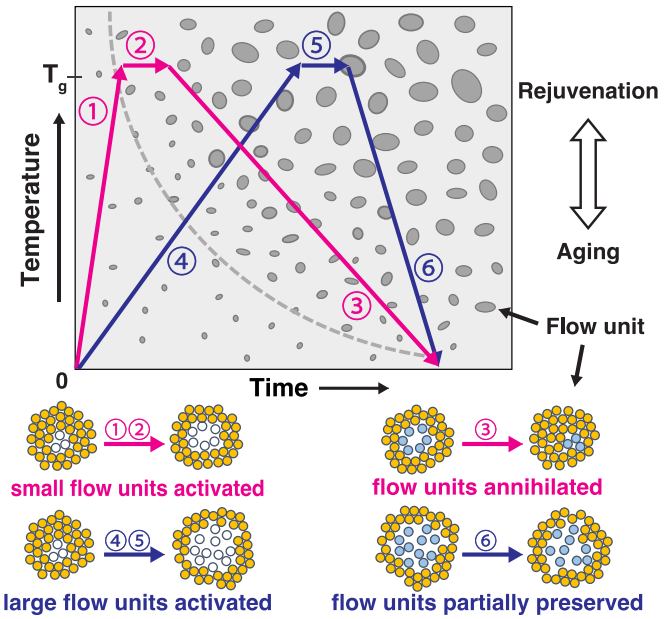

FIG. 6. Illustration of the memory effect of flow units in MGs during heat treatment. The pink path represents rapid heating followed by slow cooling, while the blue path represents slow heating followed by rapid cooling. The gray ovals denote the corresponding volumes of flow units involved in activation and annihilation processes along the heat treatment paths.

is distinct from the scenario when a higher cooling-rate heat treatment is utilized.

To further substantiate our findings regarding structural evolutions in MGs subjected to varied thermal histories, we conduct mechanical tests on MGs undergo to heat treatment paths in Fig. 2. As illustrated in Fig. 5, the elastic regime of MGs treated with a low heating rate ($r_h = 5 \times 10^{10}$ K/s and $r_c = 5 \times 10^{12}$ K/s) and a low cooling rates ($r_h = 5 \times 10^{12}$ K/s and $r_c = 5 \times 10^{10}$ K/s) are less discernible, with their curves intersecting each other more than once and both yield at ~5% strain. However, the latter exhibits the highest ultimate tensile strength along with the most rapid stress drop (see the purple curve). In contrast, the MG subjected to a longer annealing duration ($r_h = 5 \times 10^{12}$ K/s and $r_c = 5 \times 10^{12}$ K/s) distinctively shows lowest elastic modulus and ultimate strength. It is notable that all MGs subjected to heat treatment yield earlier compared to the as-cast MG.

IV. DISCUSSION

Previous research into the thermal treatment of MGs has predominantly focused on exploring the effects of annealing time and annealing temperature. In our study, we intend to underscore the importance of the heating and cooling stages preceding and following annealing. We ground this emphasis on the nonequilibrium nature of the glassy structure and structural relaxation within the fast-dynamic regime [16,18,40], as our simulations, which span from picoseconds to nanoseconds, investigate γ relaxation and fast-cage dynamics in the relaxation spectrum. These considerations will assist in interpreting several unique findings in this study.

First, the dissimilar effects of heating and cooling rates, as clearly evidenced in Table I, can be clarified through the concept of "flow units" and their activation and annihilation during heat treatment [16,41,42]. These flow units harbor local structural heterogeneities at the atomic level, wherein atoms exhibit weak bonding and form local packing with diminished density. The process of rejuvenation is tied to the activation, i.e., generation of these flow units, while aging is associated with their annihilation [16,43]. Building upon prior research on flow units associated with β relaxation [9,42], we postulate in Fig. 6 the manner in which the heat treatment process influences the flow units in MGs. Here, the term flow units serves as a more general descriptor for localized atomic rearrangement in MGs, extending beyond associations with β relaxation. They may demonstrate diverse volume, activation energy, and dependency on the initial MG structure under different relaxation modes. At lower temperatures, flow units remain inactive and in a static state. Upon heating, these units are activated through atomic reconfigurations, gradually increasing their number and size over time. Upon cooling, these units are gradually annihilated in a time-dependent process in which the most unstable "reversible" flow units are rapidly eliminated, while the more stable "irreversible" units tend to persist. While the simulation is performed within the fast-dynamics regime timescale, the observation concerning reversible and irreversible processes echoes the conclusions of Zhao *et al.* on β relaxation in MGs, wherein a unique endothermic sub-T_g peak in the differential scanning calorimetry curve marks the reversible part [17]. It may also furnish atomic-scale elucidations for the reversible and irreversible changes in thermodynamic properties observed under diverse pressures during isothermal relaxation below the T_g, as reported by Wang *et al.* [44]. From the perspective of flow units, the variations in mechanical properties of MGs illustrated

in Fig. 5 can also be interpreted. The pronounced strain-hardening effects in the MG treated with a lower cooling rate (purple curve) may be ascribed to the activation and interaction of small-sized flow units, which hinder the shear flow during deformation. Conversely, if large-sized flow units have already been activated in the MG (see green curve), they serve as preferential channels for the shear flow.

Second, we suggest that the time-dependent relaxation process gives rise to the memory effect, which has also been identified in the investigation of fast boson peak dynamics during double-step isothermal aging [15]. Figure 6 illustrates that slower heating results in the activation of larger, irreversible flow units (see path ④), while rapid heating prompts the activation of smaller, reversible flow units (see path ①). On the other hand, the reversibility of activated flow units is also dependent on the cooling rate. Slow cooling provides the required time for the activated flow units to be eliminated, thus exhibiting a less pronounced memory effect (see path ③). Fast cooling, however, limits relaxation from higher energy states and tends to preserve their structural configuration at higher temperature, leading to a more significant memory effect (see path ⑥). The energy required to activate a flow unit can be estimated based on the corresponding transition across energy barriers in the PEL [37,42,43,45]. The competing mechanism between aging and rejuvenation, i.e., between the annihilation and activation of flow units, can be inferred from the activation energy distributions presented in Fig. 4(a). Fast cooling (see pink curve) during the heat treatment process augments both the proportion of events with higher activation energy and, notably, those with lower activation energy compared to the as-cast MG, as highlighted by the dish-shaped rectangles. This suggests concurrent annihilation and activation of flow units.

Moreover, the data from Figs. 1(b) and 2(a)–2(c) indicate that when the annealing temperature is maintained slightly above the T_g of the as-cast MG, extending the annealing time throughout the entire heat treatment process could negatively affect the aging process, contingent on the initial MG structure. This can be rationalized by examining paths ② and ⑤ in Fig. 6, that isothermal annealing over short time periods does not activate flow units uniformly. Instead, a gradient distribution of activated flow-unit sizes may be produced, indicating that both reversible and irreversible flow units could be active during this stage. Meanwhile, flow units already present in MGs prior to the annealing stage, the size and distribution of which are determined by the initial MG quenching rate and heating rate, will undergo rearrangement or size expansion during annealing. Consequently, when a higher quenching rate is applied to create a less relaxed MG structure, a greater proportion of flow units will be generated. During the annealing stage, the rearrangement of these flow units tends to exceed their expansion. After sufficient cooling time, the annihilation of flow units tends to surpass their activation. This reasoning could potentially elucidate the observations reported by Wang *et al.*, where initially aged MG were rejuvenated to a degree even higher than initially rejuvenated ones [10]. In fact, we further propose that the cooling stage of the heat treatment process could be perceived as an annealing stage under gradient temperature control. As such, instead of designing a multistep heat treatment process, a desired distribution of flow units, and thereby the balance between aging and rejuvenation, could be possibly attained by carefully adjusting the maximum temperature and cooling rate, as implied by path ③ in Fig. 6.

Additionally, we would like to highlight the related phenomenological concept of "cages." Cages are used to describe the local atomic environment, in contrast to flow units. As shown in Fig. 3, the results reveal a second peak in the displacement-magnitude distribution. We propose that this peak is associated with the radius of the cage, a key aspect to comprehend the caging effects in MGs. Earlier research has shown that the rapid dynamics within these cages continues at all temperatures, without a specific timescale [9,18,34,46]. By combining the understanding of both flow units and cages, future research could potentially provide greater insights into the swift dynamics during the relaxation process of MGs.

V. CONCLUSIONS

In summary, this work delves into the structural relaxation of MGs in the fast-dynamic regime when exposed to varied thermal histories. We find that the impact of heating rate is greatly tied to the initial MG state, while a slower cooling rate consistently promotes MG aging. Extending the annealing duration brings about a subtle interplay in the MG structural relaxation, resulting in either aging or rejuvenation, depending on their specific thermal history. The memory effect, facilitated by the reversible (irreversible) activation and annihilation of flow units in MGs, offers a rationale for the disparate influences of heating and cooling rates during the heat treatment process. By considering the cooling stage as a gradient temperature-controlled annealing phase, we demonstrate that desired active-flow unit distributions can be achieved by adjusting its rate. This research reveals significant atomic-scale insights, particularly through the lens of flow units and fast-cage dynamics for developing effective heat treatment strategies to fine-tune MG structures.

ACKNOWLEDGMENTS

This work is supported by the U.S. Department of Energy (DOE), Office of Science, Office of Basic Energy Sciences, under Award No. DE-SC0020295. A part of S.Y.'s work was performed under the auspices of the U.S. DOE at Lawrence Livermore National Laboratory under Contract No. DE-AC52-07NA27344. The authors acknowledge the Center for Advanced Research Computing (CARC) at the University of Southern California for providing computing resources that have contributed to the research results reported within this paper.

[1] K. Albe, Y. Ritter, and D. Şopu, Enhancing the plasticity of metallic glasses: Shear band formation, nanocomposites and nanoglasses investigated by molecular dynamics simulations, Mech. Mater. **67**, 94 (2013).

[2] L. Tian, Y.-Q. Cheng, Z.-W. Shan, J. Li, C.-C. Wang, X.-D. Han, J. Sun, and E. Ma, Approaching the ideal elastic limit of metallic glasses, Nat. Commun. **3**, 609 (2012).
[3] J. Schroers and W. Johnson, Ductile bulk metallic glass, Phys. Rev. Lett. **93**, 255506 (2004).
[4] W. H. Wang, Bulk metallic glasses with functional physical properties, Adv. Mater. **21**, 4524 (2009).
[5] Q. Zheng, Y. Zhang, M. Montazerian, O. Gulbiten, J. C. Mauro, E. D. Zanotto, and Y. Yue, Understanding glass through differential scanning calorimetry, Chem. Rev. **119**, 7848 (2019).
[6] V. M. Giordano and B. Ruta, Unveiling the structural arrangements responsible for the atomic dynamics in metallic glasses during physical aging, Nat. Commun. **7**, 10344 (2016).
[7] P. Luo, M. X. Li, H. Y. Jiang, P. Wen, H. Y. Bai, and W. H. Wang, Temperature dependent evolution of dynamic heterogeneity in metallic glass, J. Appl. Phys. **121**, 135104 (2017).
[8] M. Zhang, Y. M. Wang, F. X. Li, S. Q. Jiang, M. Z. Li, and L. Liu, Mechanical relaxation-to-rejuvenation transition in a Zr-based bulk metallic glass, Sci. Rep. **7**, 625 (2017).
[9] W. H. Wang, Dynamic relaxations and relaxation-property relationships in metallic glasses, Prog. Mater. Sci. **106**, 100561 (2019).
[10] M. Wang, S. Lü, S. Wu, and W. Guo, Rejuvenation behavior and microstructural evolution of Cu-Zr metallic glass during multiple recovery annealing treatment via molecular dynamic simulation, J. Alloys Compd. **945**, 169294 (2023).
[11] Y. Q. Cheng, H. W. Sheng, and E. Ma, Relationship between structure, dynamics, and mechanical properties in metallic glass-forming alloys, Phys. Rev. B **78**, 014207 (2008).
[12] F. Zhang, M. I. Mendelev, Y. Zhang, C.-Z. Wang, M. J. Kramer, and K.-M. Ho, Effects of sub-T_g annealing on $Cu_{64.5}Zr_{35.5}$ glasses: A molecular dynamics study, Appl. Phys. Lett. **104**, 061905 (2014).
[13] H. Bin Yu, W. H. Wang, H. Y. Bai, and K. Samwer, The β-relaxation in metallic glasses, Natl. Sci. Rev. **1**, 429 (2014).
[14] Q. Wang, J. Ding, L. Zhang, E. Podryabinkin, A. Shapeev, and E. Ma, Predicting the propensity for thermally activated β events in metallic glasses via interpretable machine learning, npj Comput. Mater. **6**, 194 (2020).
[15] P. Luo, Y. Z. Li, H. Y. Bai, P. Wen, and W. H. Wang, Memory effect manifested by a boson peak in metallic glass, Phys. Rev. Lett. **116**, 175901 (2016).
[16] Z. Lu, B. S. Shang, Y. T. Sun, Z. G. Zhu, P. F. Guan, W. H. Wang, and H. Y. Bai, Revealing β-relaxation mechanism based on energy distribution of flow units in metallic glass, J. Chem. Phys. **144**, 144501 (2016).
[17] R. Zhao, H. Y. Jiang, P. Luo, L. Q. Shen, P. Wen, Y. H. Sun, H. Y. Bai, and W. H. Wang, Reversible and irreversible β -relaxations in metallic glasses, Phys. Rev. B **101**, 094203 (2020).
[18] Y.-T. Sun, R. Zhao, D.-W. Ding, Y.-H. Liu, H.-Y. Bai, M.-Z. Li, and W.-H. Wang, Distinct relaxation mechanism at room temperature in metallic glass, Nat. Commun. **14**, 540 (2023).
[19] D. Şopu, X. Yuan, F. Moitzi, M. Stoica, and J. Eckert, Structure-property relationships in shape memory metallic glass composites, Materials **12**, 1419 (2019).
[20] F. Spieckermann, D. Şopu, V. Soprunyuk, M. B. Kerber, J. Bednarčík, A. Schökel, A. Rezvan, S. Ketov, B. Sarac, E. Schafler and J. Eckert, Structure-dynamics relationships in cryogenically deformed bulk metallic glass, Nat. Commun. **13**, 127 (2022).
[21] Y. Q. Cheng and E. Ma, Atomic-level structure and structure–property relationship in metallic glasses, Prog. Mater. Sci. **56**, 379 (2011).
[22] D. Şopu, X. Yuan, and J. Eckert, Annealing metallic glasses above T_g in order to accelerate the relaxation process in molecular dynamics simulations, Appl. Phys. Lett. **120**, 011904 (2022).
[23] A. P. Thompson, H. M. Aktulga, R. Berger, D. S. Bolintineanu, W. M. Brown, P. S. Crozier, P. J. in't Veld, A. Kohlmeyer, S. G. Moore, T. D. Nguyen *et al.*, LAMMPS - a flexible simulation tool for particle-based materials modeling at the atomic, meso, and continuum scales, Comput. Phys. Commun. **271**, 108171 (2022).
[24] M. I. Mendelev, Y. Sun, F. Zhang, C. Z. Wang, and K. M. Ho, Development of a semi-empirical potential suitable for molecular dynamics simulation of vitrification in Cu-Zr alloys, J. Chem. Phys. **151**, 214502 (2019).
[25] See Supplemental Material at http://link.aps.org/supplemental/10.1103/PhysRevMaterials.7.123603 for the evolution of Cu-centered full icosahedra concentration generated at different cooling rates during quenching; comparison of predominant atomic Voronoi polyhedra distribution of as-cast metallic glasses (MGs) prepared at different quenching rates; MG potential energy and full icosahedra as a function of temperature for different heat treatment paths; pair-distribution functions of MGs treated with different thermal history; and mean-square displacement of MGs generated at different quench rates across varying temperatures.
[26] J. J. Maldonis, A. D. Banadaki, S. Patala, and P. M. Voyles, Short-range order structure motifs learned from an atomistic model of a $Zr_{50}Cu_{45}Al_5$ metallic glass, Acta Mater. **175**, 35 (2019).
[27] J. Ding, Y.-Q. Q. Cheng, and E. Ma, Full icosahedra dominate local order in $Cu_{64}Zr_{34}$ metallic glass and supercooled liquid, Acta Mater. **69**, 343 (2014).
[28] H. W. Sheng, W. K. Luo, F. M. Alamgir, J. M. Bai, and E. Ma, Atomic packing and short-to-medium-range order in metallic glasses, Nature (London) **439**, 419 (2006).
[29] S. Y. Wang, C. Z. Wang, M. Z. Li, L. Huang, R. T. Ott, M. J. Kramer, D. J. Sordelet, and K. M. Ho, Short- and medium-range order in a $Zr_{73}Pt_{27}$ glass: Experimental and simulation studies, Phys. Rev. B **78**, 184204 (2008).
[30] Z.-Y. Yang, Y.-J. Wang, and A. Zaccone, Correlation between vibrational anomalies and emergent anharmonicity of the local potential energy landscape in metallic glasses, Phys. Rev. B **105**, 014204 (2022).
[31] Y. X. Chen, S. P. Pan, X. Q. Lu, H. Kang, Y. H. Zhang, M. Zhang, S. D. Feng, K. L. Ngai, and L. M. Wang, Understanding the unusual-caged dynamics from the microstructure and interatomic interactions in binary metallic glass-forming liquids, J. Non-Cryst. Solids **590**, 121699 (2022).
[32] Z. Wang, K. L. Ngai, W. H. Wang, and S. Capaccioli, Coupling of caged molecule dynamics to Johari-Goldstein β-relaxation in metallic glasses, J. Appl. Phys. **119**, 024902 (2016).
[33] K. K. Qiu, X. D. Wang, T. D. Xu, J. Liu, Q. P. Cao, D. X. Zhang, and J. Z. Jiang, Unravelling the origin of in-cage vibrations in a $La_{50}Al_{15}Ni_{35}$ metallic glass, Mater. Today Phys. **21**, 100515 (2021).
[34] K. L. Ngai, Why the fast relaxation in the picosecond to nanosecond time range can sense the glass transition, Philos. Mag. **84**, 1341 (2004).

[35] K. L. Ngai, Interpreting the nonlinear dielectric response of glass-formers in terms of the coupling model, J. Chem. Phys. **142**, 114502 (2015).

[36] H. Bin Yu, M. H. Yang, Y. Sun, F. Zhang, J. B. Liu, C. Z. Wang, K. M. Ho, R. Richert, and K. Samwer, Fundamental link between β relaxation, excess wings, and cage-breaking in metallic glasses, J. Phys. Chem. Lett. **9**, 5877 (2018).

[37] N. Mousseau and G. T. Barkema, Traveling through potential energy landscapes of disordered materials: The activation-relaxation technique, Phys. Rev. E **57**, 2419 (1998).

[38] E. Cancès, F. Legoll, M.-C. Marinica, K. Minoukadeh, and F. Willaime, Some improvements of the activation-relaxation technique method for finding transition pathways on potential energy surfaces, J. Chem. Phys. **130**, 114711 (2009).

[39] C. Liu and Y. Fan, Emergent fractal energy landscape as the origin of stress-accelerated dynamics in amorphous solids, Phys. Rev. Lett. **127**, 215502 (2021).

[40] Z. Long, L. Kong, P. Tao, Z. Huang, X. Zhu, X. Xu, and Y. Yang, Viscosity and structure relaxation in $Zr_{60}Cu_{20}Al_{10}Ni_{10}$ metallic glass, J. Non-Cryst. Solids **604**, 122150 (2023).

[41] Z. Wang, P. Wen, L. S. Huo, H. Y. Bai, and W. H. Wang, Signature of viscous flow units in apparent elastic regime of metallic glasses, Appl. Phys. Lett. **101**, 121906 (2012).

[42] T. P. Ge, X. Q. Gao, B. Huang, W. H. Wang, and H. Y. Bai, The role of time in activation of flow units in metallic glasses, Intermetallics **67**, 47 (2015).

[43] S. T. Liu, Z. Wang, H. L. Peng, H. B. Yu, and W. H. Wang, The activation energy and volume of flow units of metallic glasses, Scr. Mater. **67**, 9 (2012).

[44] L. M. Wang, W. H. Wang, L. L. Sun, J. Zhang, and W. K. Wang, Pressure effects on irreversible and reversible contributions to the glass transition of $Pd_{39}Ni_{10}Cu_{30}P_{21}$ bulk metallic glass, Phys. Rev. B **63**, 052201 (2001).

[45] G. Hygate and M. R. J. Gibbs, Structural relaxation in metallic glasses: Reversible and irreversible changes in a two-level systems model, J. Phys. F **17**, 815 (1987).

[46] L. Larini, A. Ottochian, C. De Michele, and D. Leporini, Universal scaling between structural relaxation and vibrational dynamics in glass-forming liquids and polymers, Nat. Phys. **4**, 42 (2008).

Supplementary Materials

The effect of heat treatment paths on the aging and rejuvenation of metallic glasses

Suyue Yuan,[a,b] Aoyan Liang,[a] Chang Liu,[a] Liang Tian,[c] Normand Mousseau,[d] and Paulo S. Branicio[1a]

[a]Mork Family Department of Chemical Engineering and Materials Science, University of Southern California, Los Angeles, CA 90089, United States

[b]Materials Science Division, Lawrence Livermore National Laboratory, Livermore, CA 94550, United States

[c]Frontier Institute of Science and Technology (FIST), Xi'an Jiaotong University, Xi'an, Shaanxi 710049, China.

[d]Département de Physique, Université de Montréal, C.P. 6128, succ. Centre-ville, Montréal (Québec), Canada

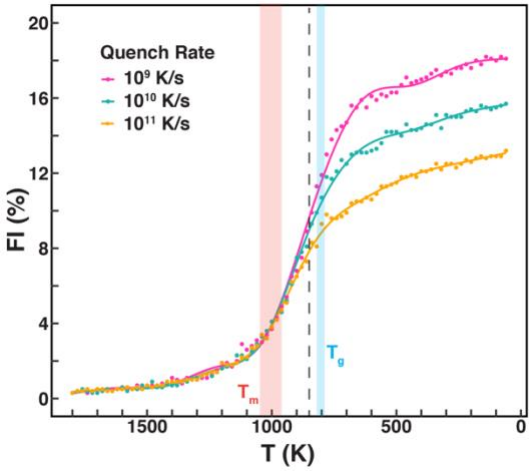

Fig. S1 Evolution of Cu centered Full Icosahedra (FI) concentration for $Cu_{64}Zr_{36}$ generated at different cooling rates during quenching. The dashed line indicates the selected annealing temperature while the shaded areas represent the range of glass transition temperature (T_g) and melting temperature (T_m) of the samples obtained using the different quench rates.

[1] branicio@usc.edu

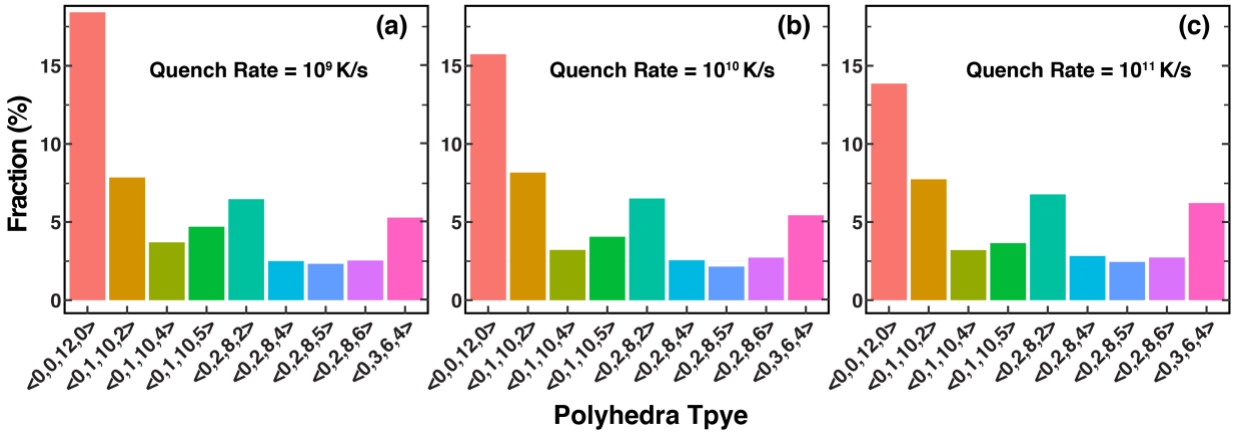

Fig. S2 Predominant atomic Voronoi polyhedra distribution of as-cast metallic glasses (MGs) prepared at quenching rates of 10^9, 10^{10}, and 10^{11} K/s, respectively.

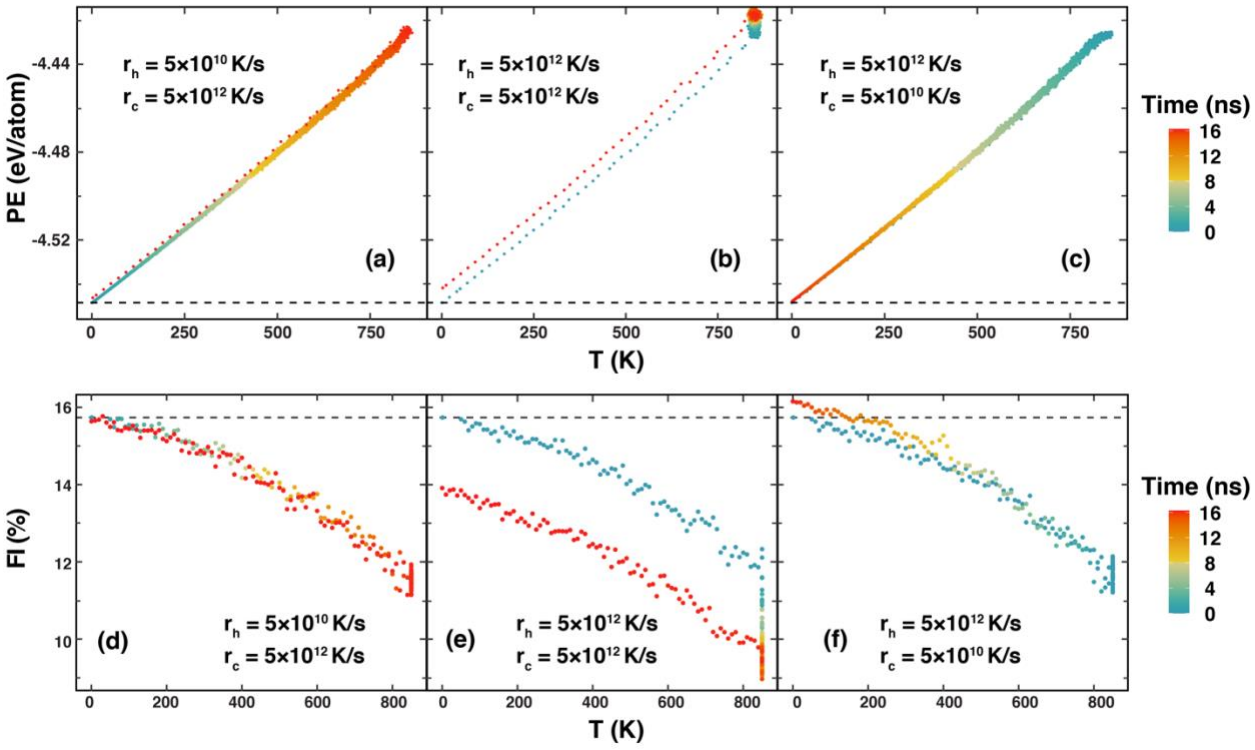

Fig. S3 MG potential energy (PE) and full icosahedra (FI) as a function of temperature for different heat treatment paths. Heating rates, r_h, and cooling rates, r_c, are indicated in each plot. All samples are generated using a quench rate of 10^{10} K/s followed by heat treatments of equal total duration.

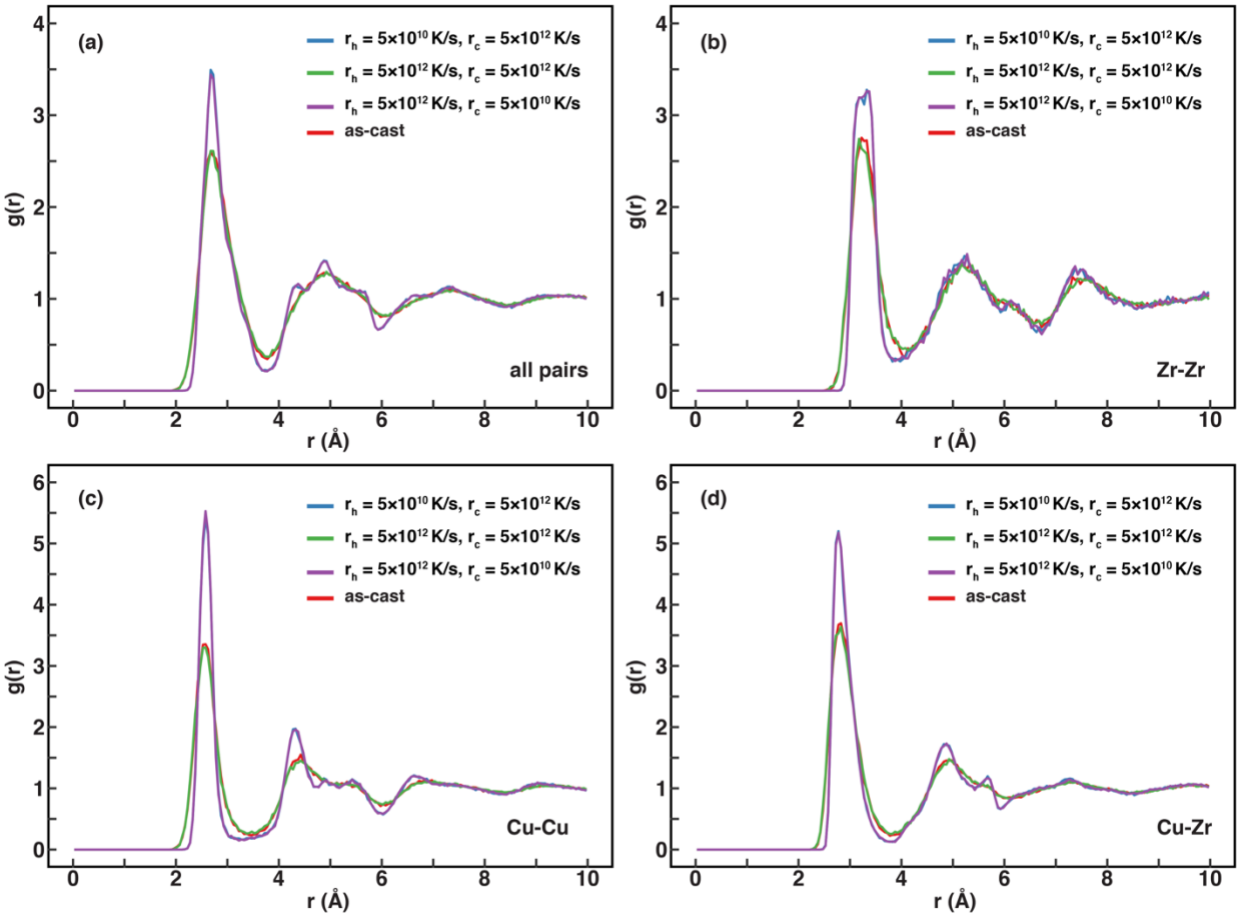

Fig. S4 Pair-distribution functions of MGs treated with different thermal history.

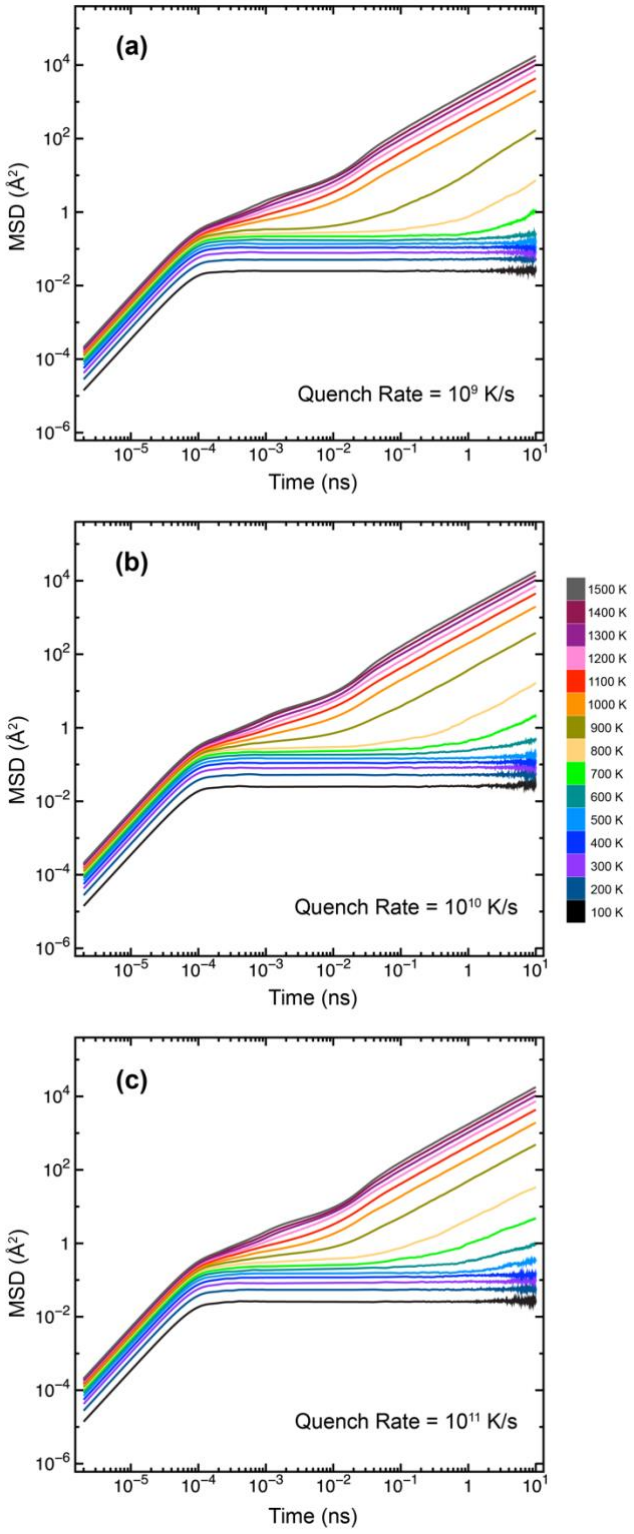

Fig. S5 Mean square displacement (MSD) of MGs generated at different quench rates across varying temperatures.